# Moisture source variations for summer rainfall in different intensity classes over Huaihe River Valley, China

Yubo Liu[1,2] · Chi Zhang[1,3] · Qiuhong Tang[1,2] · Seyed-Mohammad Hosseini-Moghari[1] ·
Gebremedhin Gebremeskel Haile[1] · Laifang Li[4,9,10] · Wenhong Li[5] · Kun Yang[6] · Ruud J. van der Ent[7] · Deliang Chen[8]

## Abstract

Rainfall is one of the most influential climatic factors on regional development and environment, and changes in rainfall intensity are of specific concern. In the Huaihe River Valley (HRV), heavy rainfall is a primary trigger of floods. However, the difference in the origin of moisture contributed to heavy rainfall and light rainfall is rarely studied and not entirely understood. This study analyzes the rainfall moisture sources in association with different categories of rainfall intensity over the HRV during 1980–2018 using the Water Accounting Model with ERA-Interim reanalysis and precipitation observations from China Meteorological Administration. The results show that the moisture for the HRV summer rainfall is mainly from terrestrial subregion (40%), the Indian Ocean (27%), the Pacific Ocean (25%), and the local HRV (8%). In addition, moisture sources differ substantially between light and heavy rainfall. Specifically, the local HRV contributes more moisture to light rainfall (12%) compared to heavy rainfall (4%), whereas the Indian Ocean contributes more to heavy rainfall (33%) than to light rainfall (20%). The grids located in the southern source region make higher contribution ratio in heavy rainfall than in light rainfall. These results suggest that moisture from distant oceanic areas, especially the Indian Ocean, plays a crucial role in intense summer rainfall, whereas moisture from the land sources covering local grids plays a dominant role in light rainfall in the HRV.

✉ Qiuhong Tang
tangqh@igsnrr.ac.cn

1   Key Laboratory of Water Cycle and Related Land Surface Processes, Institute of Geographic Sciences and Natural Resources Research, Chinese Academy of Sciences, Beijing, China

2   University of Chinese Academy of Sciences, Beijing, China

3   Key Laboratory of Land Surface Pattern and Simulation, Institute of Geographic Sciences and Natural Resources Research, Chinese Academy of Sciences, Beijing, China

4   Department of Meteorology and Atmospheric Science, The Pennsylvania State University, University Park, PA 16802, USA

5   Earth and Ocean Sciences, Nicholas School of the Environment and Earth Sciences, Duke University, Durham, USA

6   Ministry of Education Key Laboratory for Earth System Modeling, Department of Earth System Science, Tsinghua University, Beijing 100084, China

7   Department of Water Management, Faculty of Civil Engineering and Geosciences, Delft University of Technology, Delft, The Netherlands

8   Regional Climate Group, Department of Earth Sciences, University of Gothenburg, Gothenburg, Sweden

9   Institute of Computational and Data Sciences, the Pennsylvania State University, University Park, PA 16802, USA

10  Earth and Environmental Systems Institute, The Pennsylvania State University, University Park, PA 16802, USA

# 1 Introduction

The Huaihe River Valley (HRV), located in eastern China (30.5–36.5° N, 111.5–121° E), is a key agricultural region in China playing a vital role in ensuring food security, economic development and ecological stability (Gao et al. 2008). However, the agriculture and economy have been severely affected by flooding events largely caused by heavy rainfall events in summer (Hao and Zhao 2014; Zhang and You 2014). With the uncertain future changes in rainfall over the HRV, these effects are still difficult to predict and minimize.

Rainfall is considered as a key meteorological parameter and plays a significant role in the hydrological process. Many existing studies provide a comprehensive understanding of the HRV rainfall in the fields of meteorology and hydrology. From a meteorological perspective, it has been confirmed that sea surface temperature (SST) anomalies and the related variation of important climate modes, such as El Niño Southern Oscillation (ENSO), Pacific Decadal Oscillation (PDO) and Indian Ocean Dipole (IOD), have an impact on the intensity and variations of HRV summer rainfall (Li et al. 2016; Wang et al. 2016). From a hydrological perspective, moisture source, water vapor uplift and transport driven by atmospheric circulations are the focus of attention (Gustafsson et al. 2010; Jiang et al. 2017; Pathak et al. 2016; Zhou and Yu 2005). The large amount of moisture from the Indian Ocean and Pacific Ocean carried by the Asian summer monsoon and the local recycling are believed to feed HRV rainfall. (Ding and Chan 2005; Guo et al. 2018; Huang et al. 2004).

Identifying moisture sources for regional rainfall can help understand the hydrological linkage between the target region and the moisture contributing region (Trenberth et al. 2010), and this becomes increasingly important as the regional water cycle are often driven by global change factors in the Anthropocene (Findell et al. 2019; Gimeno et al. 2013; Tang, 2020). Many methods have been carried out to identify moisture source of rainfall, including analysis of the isotopic composition (Liu et al. 2007), moisture tracking based on Eulerian (Insua-Costa and Miguez-Macho 2018; van der Ent and Savenije 2011) and Lagrange algorithms (Drumond et al. 2011; Stohl and James 2002, 2005). These tools are considered to be mature and reliable, which have been widely applied to global (Gimeno et al. 2020a, b) or regional precipitation (Zhang et al. 2017, 2019).

For the HRV, Zhou and Yu (2005) illustrated that the moisture for rainfall may originate from the adjacent subtropical Pacific, the East China Sea, and the South China Sea. According to the research on the global oceanic moisture sources (Nieto et al. 2019), HRV is located in the sink

region from the North Pacific, Zanzibar Current and Arabian Sea. In addition, the importance of the land region in East Asia as a moisture source was emphasized (Fremme and Sodemann 2019). Although these studies have provided important understanding of the moisture origins of HRV rainfall, most of them focused on moisture source of mean seasonal and annual rainfall or heavy rainfall events. Few studies have investigated the moisture source differences among different rainfall intensities, i.e., light, moderate, and heavy rainfalls. Thus, it remains unclear whether moisture sources differ among the different categories of rainfall. The rule-of-thumb of atmospheric moisture balance suggests that larger amount of moisture is required in order to generate and sustain each single heavy rainfall event than light rainfall event. From this perspective, the following issues remain to be solved. Is the larger moisture demand for heavy rainfall events fulfilled by the increment of local recycling, or is it more likely to be met by the moisture evaporated from remote regions? Could the different rainfall categories be related to different moisture sources and moisture transport pathway? How does the evaporation from land and ocean, respectively, contribute to HRV rainfall? Answers to these questions are key to understand the linkages between local rainfall intensities and moisture sources, and to improve the prediction of extreme rainfall and consequent flooding events in the HRV (Li et al. 2012; Wu and Yan 2013). Therefore, the aim of this study is to investigate the contribution of moisture source for rainfall in different intensity classes over the HRV and to quantify the differences among the rainfall intensities.

The paper is organized as follows. Following this introduction, data and methods are described in Sect. 2. Section 3 presents the results, followed by a discussion in Sect. 4. Concluding remarks and limitations of this work are presented in Sect. 5.

# 2 Study area, data and methodology

## 2.1 Study area

The HRV is located in the climatic transition zone between the dry North and humid South China, with an area of about $270 \times 10^3$ km$^2$ and altitudes of 600–1000 m. It belongs to the warm temperate semi-humid monsoon climate. The annual rainfall of the study area ranges from about 500 to 1500 mm (Fig. 1). The HRV summer season extends from June to August (JJA) (Li et al. 2016), with the peak rainfall month in July (Nieto et al. 2019).

The study area (Fig. 1) is extracted from the 1.5-degree land-sea mask to represent the HRV in the reanalysis grids and includes parts of four provinces of Shandong, Henan,

**Fig. 1** The climatology of annual rainfall from CMA and the location of the HRV. The red outlined area delineates the study area and geographic location of the HRV is shown by the black outline. The inner plot shows the 1980–2018 climatology of monthly precipitation over the HRV
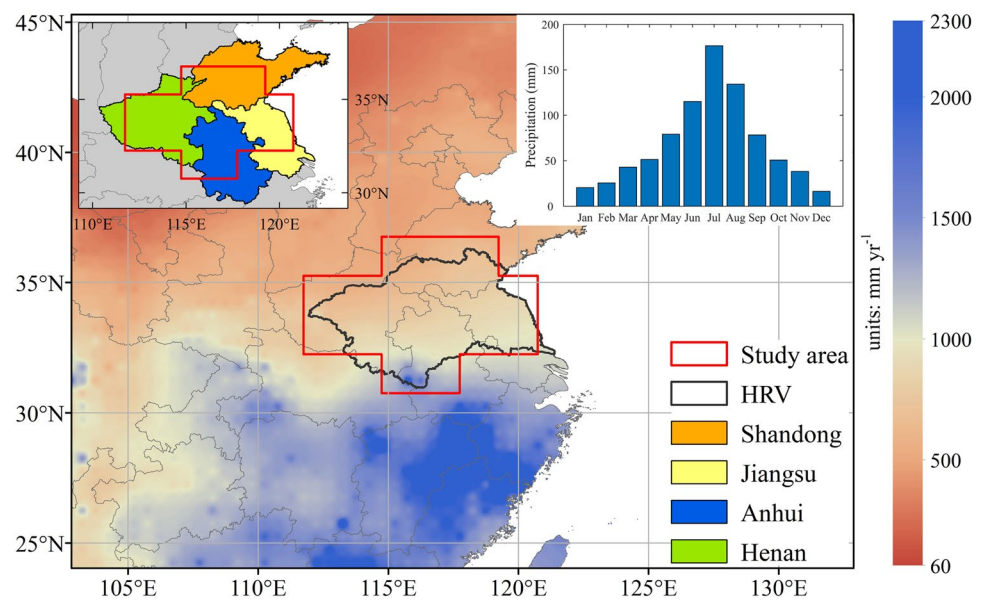
Anhui and Jiangsu in China. The rainfall in the red outlined area is extracted and the source of moisture supplied to it will be identified.

## 2.2 Data

As a quality controlled global atmospheric reanalysis product (Dee et al. 2011), the ERA-Interim (ERA-I) dataset from the European Centre for Medium-Range Weather Forecast (ECMWF) is used in this study. The data including 3-hourly precipitation and evaporation, and 6-hourly specific humidity, wind velocity and surface pressure in the lowest 23 vertical levels (200–1000 hPa), are used as the input variables for moisture tracking. In the model calculation process, these data are linearly interpolated to the time resolution of 0.5 h to maintain numerical stability (van der Ent and Savenije 2011; van der Ent et al. 2010, 2013). The vertical integral of water vapor flux is used for analysis and discussion. The ERA-I data used in this study covers the period from 1980 to 2018 with the spatial resolution of $1.5° \times 1.5°$.

Compared to other global reanalysis data, ERA-I data shows smaller residuals in the global hydrological budget (Trenberth et al. 2011). Its precipitation data is derived from the forecast model, and the accuracy is affected by the model physics (Dee et al. 2011). Considering that the accuracy of precipitation data is very important to this study, a set of observed precipitation data is used to verify the ERA-I precipitation data. The observed daily precipitation dataset (V2.0) is obtained from the National Meteorological Information Center, China Meteorological Administration (CMA) (Zhao et al. 2014). This dataset covers the period from 1980 to 2018 with the spatial resolution of $0.5° \times 0.5°$.

## 2.3 Methodology

### 2.3.1 Rainfall intensity classes

The definition of rainfall intensity class in this study combines the rainfall on the basin scale and the rainfall on the grid scale. This definition considering two spatial scales is to avoid the neglection of rainfall events that have a large difference between the grid precipitation and the average value over the whole basin, which could result in the mismatch of daily rainfall intensity categories. On the basin scale, American Meteorological Society (AMS) Glossary of Meteorology (light rainfall: $< 6$ mm day$^{-1}$; moderate rainfall: 6–18 mm day$^{-1}$; heavy rainfall: $> 18$ mm day$^{-1}$) is considered. On the grid scale, the two critical values refer to the upper limit of light-moderate rainfall transition range (17 mm day$^{-1}$) and heavy rainfall (50 mm day$^{-1}$) in the CMA rainfall intensity classification criteria (light rainfall: $< 17$ mm day$^{-1}$; moderate rainfall: 17–50 mm day$^{-1}$; heavy rainfall: $> 50$ mm day$^{-1}$). In summary, the definitions of rainfall intensity classes in this study are described as follows: the heavy rainfall class is that the average precipitation over HRV is more than 18 mm day$^{-1}$, or the precipitation in a single grid is more than 50 mm day$^{-1}$; the light rainfall class is that the average precipitation over HRV less than 6 mm day$^{-1}$, and the precipitation in each grid is less than 17 mm day$^{-1}$; the rest has been classified as the moderate rainfall.

### 2.3.2 Water Accounting Model

Water Accounting Model (WAM) is used to investigate the moisture source of rainfall over the HRV. WAM is

a moisture tracing model based on the Euler framework, which can quantify the source and sink relationship through both forward and backward calculation (van der Ent and Savenije 2011; van der Ent et al. 2010, 2013). The validity and consistency of the forward and backward algorithm of WAM have been verified through numerical experiments and theoretical derivation (Zhang and Li 2014).

The basic and premise of WAM algorithm is the atmospheric moisture balance and the assumption of a well-mixed atmosphere (Goessling and Reick 2013). It assumes that the precipitation probability of both the water molecules evaporated from the inside of the grid and the advected water molecules evaporated from the other grids is same. This implies that the ratio of advected and evaporated water molecules remains the same in both evaporation and the precipitable water (Burde 2010). The relationship can be described by the mixing ratio $R$,

$$R = \frac{E_r}{E} = \frac{W_r}{W} \tag{1}$$

where $E$ is total evaporation and $W$ is precipitable water of each grid, $W_r$ and $E_r$ represent the precipitable water and evaporation from the source region $r$. Using this assumption, the atmospheric moisture equation can be applied to a certain source region as given in the following relationship,

$$\frac{\partial W_r}{\partial t} + \frac{\partial (W_r u)}{\partial x} + \frac{\partial (W_r v)}{\partial y} = E_r - P_r \tag{2}$$

where $W_r$, $E_r$ and $P_r$ represent the precipitable water, evaporation and precipitation from the source region, respectively; $u$ and $v$ are the wind velocity on the zonal ($x$) and meridional ($y$) direction. It is worth noting that the moisture contribution calculated by WAM refers to the moisture evaporated from the region without considering advection.

The traceback duration of the daily rainfall in WAM was set to 20 days, which is longer than the proposed atmospheric moisture residence time of approximately one week to 10 days (Bosilovich 2002; Trenberth 1998, 1999; Yoshimura et al. 2004). This setting ensures that more than 85% of the rainfall moisture can be allocated to sources. In this study, we pay special attention to the regions with relatively high contribution to the precipitation over the study area, and temporarily ignore the rest grids which are far away from study area with extremely rare contribution on the global scale. Thus, the main moisture source region is defined, in which the cumulative climatology of JJA moisture contribution in all the grids of the source region accounts for 90% of the total. For the different intensity rainfall, the contribution is separately summed up according to the rainfall intensity classes to generate spatial maps of moisture contribution to the rainfall in the target area.

### 2.3.3 Method

The root mean square error (RMSE), correlation coefficient (CC) and relative bias (RBias) are used to assess the difference between CMA and ERA-I precipitation data as shown in the following calculation, where $n$ is the total number of grids in the study area.

$$RMSE = \sqrt{\frac{\sum_{i=1}^{n}(P_{ERA,i} - P_{CMA,i})^2}{n}} \tag{3}$$

$$CC = \frac{\sum_{i=1}^{n}(P_{ERA,i} - \overline{P_{ERA}})\left(P_{CMA,i} - \overline{P_{CMA}}\right)}{\sqrt{\sum_{i=1}^{n}\left(P_{ERA,i} - \overline{P_{ERA}}\right)^2}\sqrt{\sum_{i=1}^{n}\left(P_{CMA,i} - \overline{P_{CMA}}\right)^2}} \tag{4}$$

$$RBias = \frac{\sum_{i=1}^{n}(P_{ERA,i} - P_{CMA,i})}{\sum_{i=1}^{n}P_{ERA,i}} \tag{5}$$

In order to compare the moisture contribution of a grid or subregion in different intensity classes, the contribution ratio is used to quantify the proportion of grid or subregion contribution to the rainfall. The contribution ratio ($R_c$) can be calculated as the following formula, where $E_{r,i}$ represents the volume of moisture contribution from each grid (or each subregion) in the main moisture source region. In addition, the Student t-test is used for testing the significance of differences between categories.

$$R_c = \frac{E_{r,i}}{\sum_{i=1}^{n}E_{r,i}} \times 100\% \tag{6}$$

## 3 Results

### 3.1 Performance of ERA-I rainfall over the HRV

The performance and variations of ERA-I rainfall are shown in Fig. 2 as compared with CMA data. The climatology of summer rainfall over the HRV from CMA and ERA-I is 426.0 mm JJA$^{-1}$ and 443.2 mm JJA$^{-1}$, respectively. The spatial distributions of climatological JJA rainfall obtained from the two datasets are shown in Fig. 2a, b. The distribution of ERA-I is generally consistent with CMA, indicating that JJA rainfall increases from northwest to southeast of HRV. However, as compared with CMA, the ERA-I shows an overestimation in the west HRV, while there is an underestimation in the south HRV. Compared with the 0.5-degree CMA data, the lower spatial resolution of the ERA-I results in the data being calculated on a
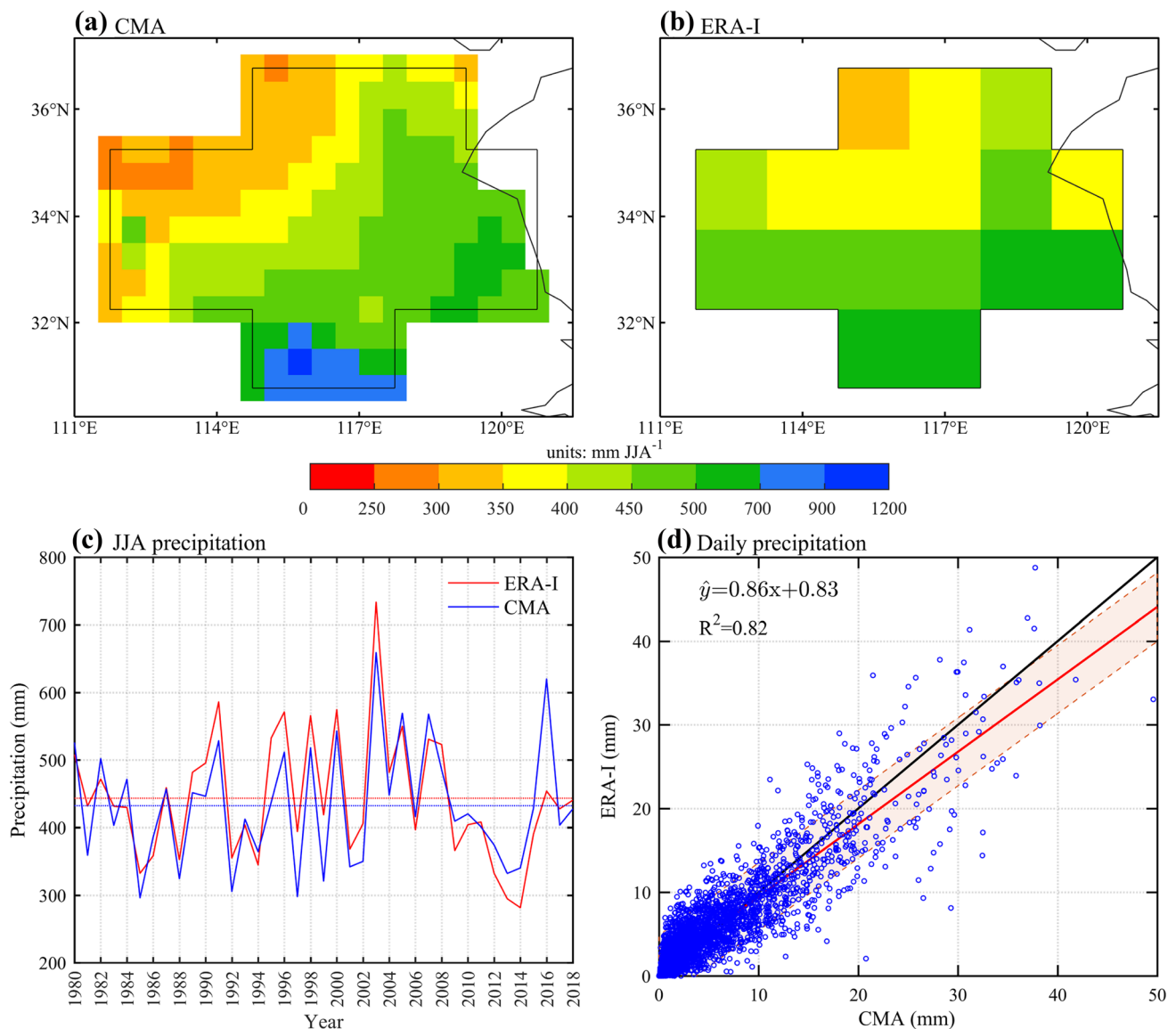
**Fig. 2** The spatial distributions of climatological JJA rainfall calculated from CMA (**a**) and ERA-I (**b**) from 1980 to 2018. **c** Time series of JJA rainfall of ERA-I (red lines) and CMA (blue lines) from 1980 to 2018. **d** Scatter plot of daily CMA vs ERA-I rainfall. The black and red lines indicate the 1:1 slope and the best fit regression line, and the shading represents the 90% credible interval

larger area and thus becomes homogenized, which is one of the important reasons for the deviation of its extreme values. In terms of the deviation from CMA observed data, ERA-I data performs well in the annual JJA rainfall with RMSE of 52.8 mm and RBias of 2.6%. The interannual variations of CMA and ERA-I precipitation in Fig. 2c are basically consistent with CC of 0.84. The scatter plot of daily precipitation (Fig. 2d) indicates that ERA-I rainfall is close to CMA data on the daily scale and the linear fitting has high statistical reliability. In addition, according to the definition of each rainfall intensity class mentioned above, the average rainfall of different intensities of ERA-I is about 107.0 mm for light rainfall, 206.2 mm for moderate rainfall and 130.0 mm for heavy rainfall, accounting for 24.1%, 46.5% and 29.4%, respectively.

## 3.2 Moisture contribution for different rainfall intensities

Figure 3 shows the spatial distribution of moisture contribution from each grid to the mean JJA rainfall in the target region, namely HRV. All color-marked grids within the red outline constitute the main moisture source region. This region ranges from 40 to 180° E and 20° S to 56° N across the equator, accounting for about 90% of the global total moisture contribution. It indicates that JJA rainfall over the

**Fig. 3** Climatology of the moisture contribution to the JJA rainfall over the HRV. The outer red lines enclose the main moisture source region. The main moisture source region is divided into four subregions: the local HRV enclosed by the black lines, the terrestrial subregion excluding the HRV (TS), the Indian Ocean (IO) and the Pacific Ocean (PO) divided by the inner red lines. The shading indicates how much evaporation each square with an area of 1.5° × 1.5° contributes to HRV rainfall
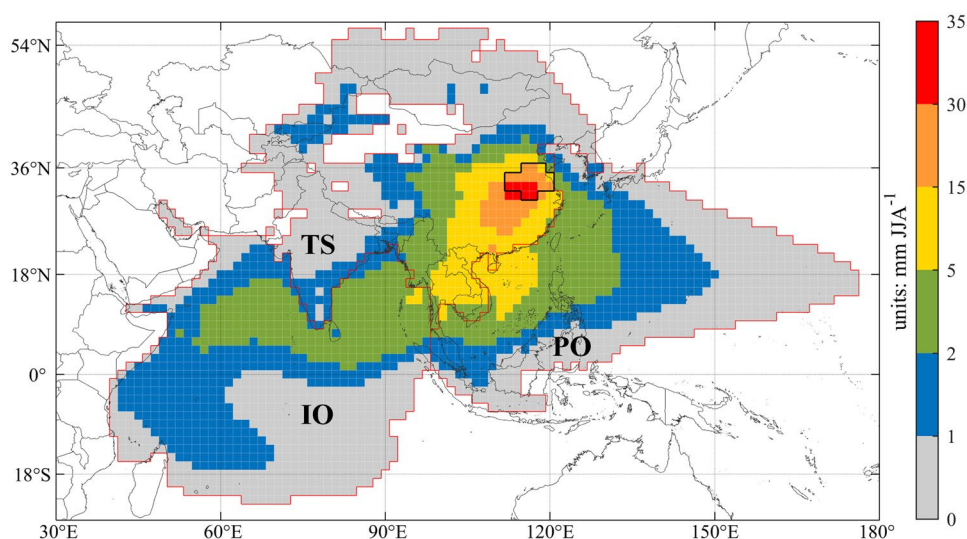
**Table 1** The mean moisture contribution ratio of each subregion to the rainfall in different intensity classes

| Classes | HRV (%) | Terrestrial subregion (%) | Indian Ocean (%) | Pacific Ocean (%) |
|---|---|---|---|---|
| Light | 11.7 | 42.9 | 19.8 | 25.6 |
| Moderate | 7.4 | 39.3 | 27.0 | 26.3 |
| Heavy | 4.1 | 39.5 | 33.0 | 23.4 |
| JJA average | 7.5 | 40.2 | 27.0 | 25.3 |

HRV is supplied mainly by the moisture from local as well as remote terrestrial and ocean areas. This distribution is consistent with the earlier study by Jiang et al. (2013). The figure clearly shows that the contribution from each grid is affected by distance. The grids with the largest moisture contribution are located in the southwest of HRV and contribute more than 30 mm of evaporation. The remote source grids on the suburb of the main source region marked in gray contribute less than 1 mm of evaporation.

To promote further quantification and analysis, the main moisture source region is partitioned. Firstly, the moisture sources are separated into land and ocean. On average, moisture originated from the land and the ocean basically breaks even, contributing about half of the tracked precipitation moisture, with 47.7% from the continent and 52.3% from the ocean to be specific. Secondly, to highlight the local role of HRV and different oceans, the main moisture source region is separated into four subregions, i.e., the local HRV, the terrestrial subregion (excluding the HRV), the Indian Ocean and the Pacific Ocean (the data presented afterward are in the same order). The moisture supply from these four subregions accounts for 7.5%, 40.2%, 27.0% and 25.3% of the overall moisture contribution from the main source region (Table 1). Converting these contributions into the HRV

rainfall, the four subregions provide 25.6 mm, 138.3 mm, 92.9 mm, and 86.9 mm rainfall, respectively.

The specific results of four subregions in Table 1 compare the contribution from the same source to different intensity rainfall classes. For each category of HRV rainfall, the proportion of contributed moisture from terrestrial subregion is the largest, about 39.3–42.9% with little change. The moisture contributed from the Pacific Ocean accounts for 23.4–26.3% with no clear regularity or significant changes in different categories. The other two subregions, the local HRV and the Indian Ocean, present obvious differences. The local HRV contributes 11.7%, 7.4% and 4.1% to light, moderate and heavy rainfall, respectively, which indicates that the heavier rainfall intensity in these three categories, the smaller its proportion. In contrast, the portion of moisture contributed from the Indian Ocean accounts for 19.8% of light rainfall, followed by 27.0% of moderate rainfall, and the largest proportion of 33.0% for heavy rainfall.

Figure 4 shows the distribution of the moisture contribution (the left column) and the corresponding ratio (the right column) of each source grid to different intensity classes. To facilitate the comparison of the differences in all intensity classes, the range of the main moisture contribution region delineated by the outer red line in Fig. 4 is still consistent with Fig. 3. The extension of the blue and green grids over the Arabian Sea and the Bay of Bengal clearly shows that the Indian Ocean contributes more and occupies a higher portion of moisture contribution to moderate and heavy rainfall than to light rainfall. However, the absence of red grids and rare orange grids in the Fig. 4e, f proves that the moisture contributed from the HRV grids and their ratios of heavy rainfall are less than those of moderate or light rainfall. These differences indicate that the distribution of moisture contributed to light rainfall is concentrated in local and adjacent area, while distribution of the origin of heavy
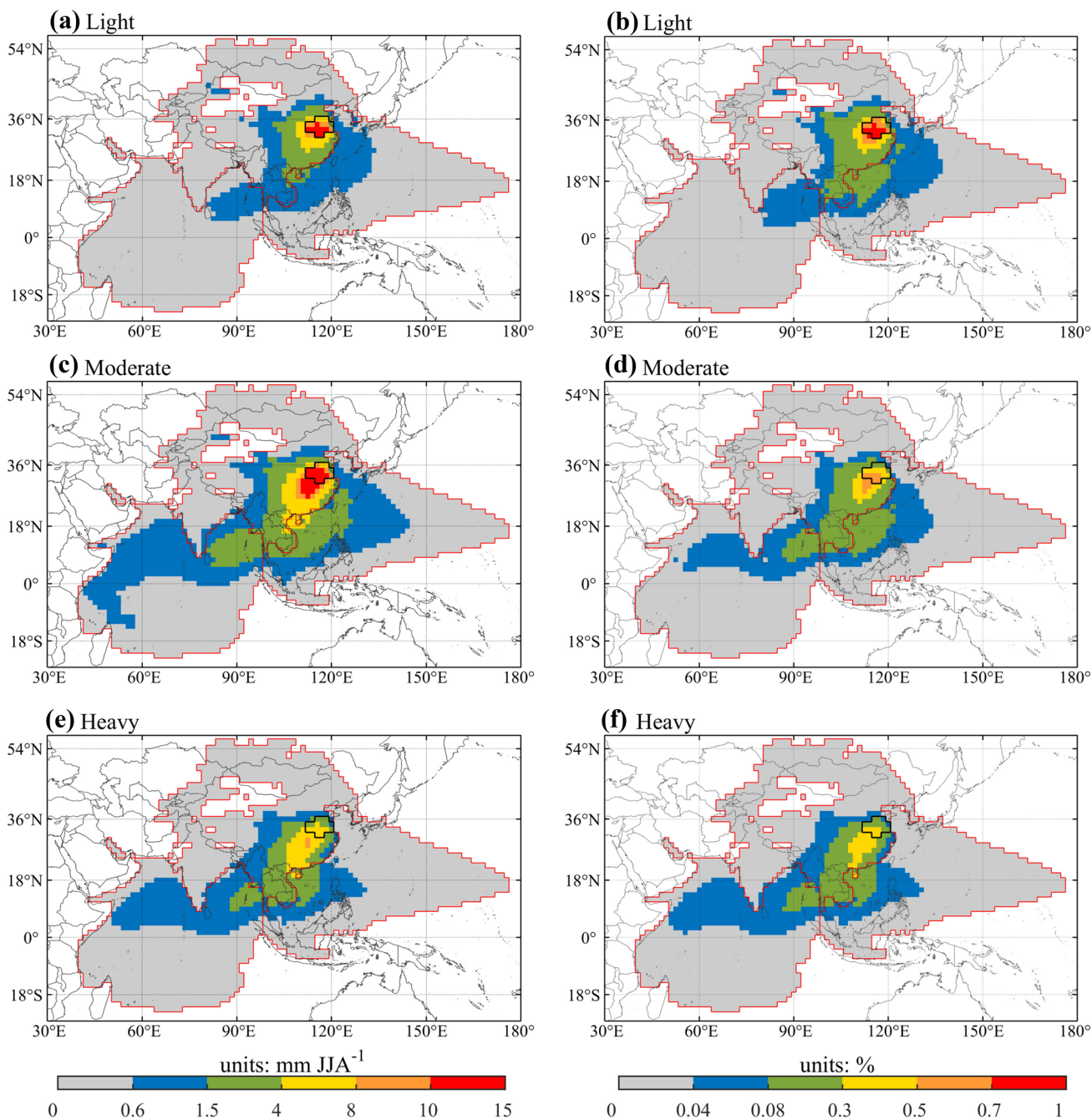
**Fig. 4** Spatial distributions of climatological moisture contributions to different JJA HRV rainfall classes and their contribution ratios for light (**a**, **b**), moderate (**c**, **d**) and heavy (**e**, **f**) rainfall

rainfall shows the extension to the ocean to obtain more moisture contribution.

### 3.3 Difference in contribution ratio between heavy rainfall and light rainfall

A comparison of the difference between the contribution of heavy rainfall and light rainfall in each subregion

and their respective interannual variations are shown in Fig. 5. Compared with portion contributed by local HRV to heavy rainfall, the moisture contributed from this region for light rainfall occupies a larger proportion. Conversely, in most years, the portion of moisture contribution from Indian Ocean for heavy rainfall is higher than that for light rainfall. The mean contribution ratios of the evaporated moisture from both local HRV and the Indian
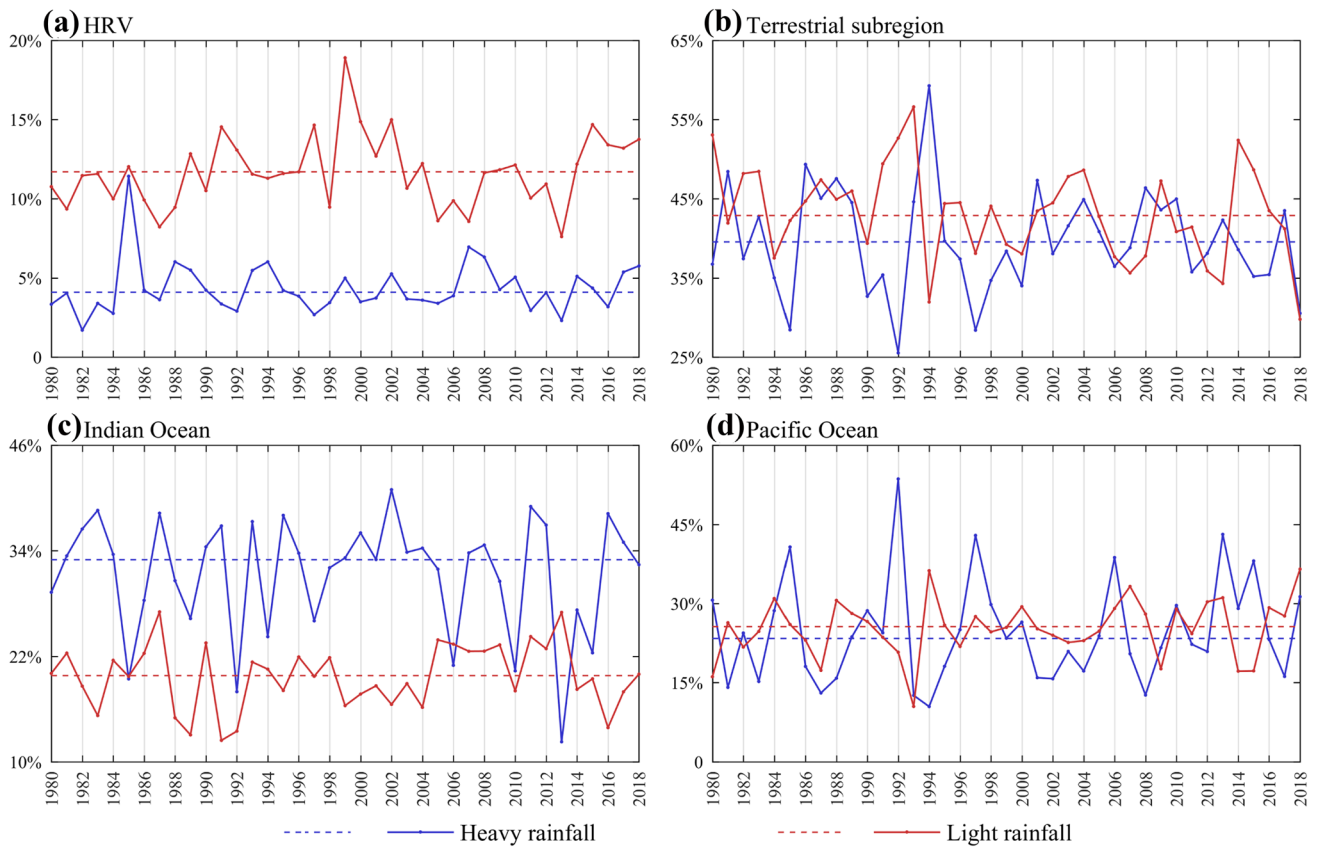
**Fig. 5** Interannual variation of the contribution ratio of evaporated moisture from the local HRV (**a**), the terrestrial subregion (**b**), the Indian Ocean (**c**) and the Pacific Ocean (**d**). The solid lines indicate the contribution ratio of each subregion to heavy rainfall (blue) or light rainfall (red) over HRV, while the dashed lines indicate the mean moisture contribution ratio of heavy rainfall (blue) or rainfall light (red)

Ocean are significantly different between heavy rainfall and light rainfall ($p < 0.05$, Student t-test). However, for the terrestrial subregion and the Pacific Ocean, the large

interannual variability of the contribution ratios of their evaporated moisture makes the differences between heavy rainfall and light rainfall insignificant.

**Fig. 6** Spatial distribution of the differences in contribution ratio between heavy and light rainfall. The shading indicates the difference in the climatology of contribution ratio between heavy rainfall and light rainfall (heavy minus light, unit: %). Vectors are the climatological 850-hPa wind (unit: m s$^{-1}$) and the contours are the climatological 850-hPa specific humidity (unit: g kg$^{-1}$). The difference in the grid with green asterisk is significant at 0.05 level of Student t-test
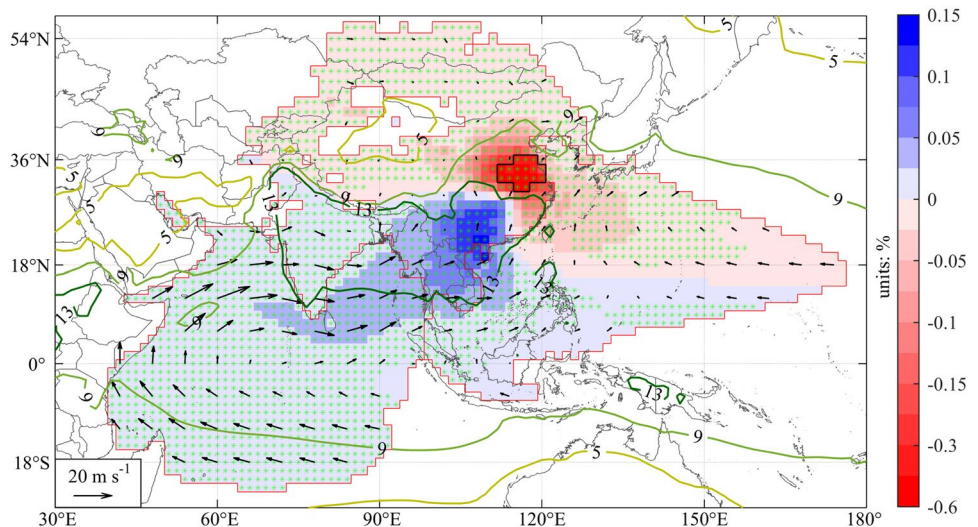
Figure 6 is the result of the Fig. 4f minus Fig. 4b, which directly shows the comparison of the grid contribution ratio between light rainfall and heavy rainfall. The red grids with negative value in the north, covering the HRV, the Pacific Ocean north of about 15° N and the terrestrial subregion north of about 30° N, have higher contribution ratios to light rainfall than to heavy rainfall, with the greatest difference located in the HRV. On the contrary, the grids in the south part with positive values have higher contribution ratio to heavy rainfall than light rainfall, indicating that they play a more important role during heavy rainfall. This explains that for the terrestrial subregion and the Pacific Ocean, the insignificant difference in the contribution ratios is due to the counterbalance of the positive value in the south and the negative value in the north. The distribution of this difference is not random. Most grids in the figure are marked with asterisks, indicating that the differences in the moisture contribution ratios of these grids are statistically significant ($p < 0.05$, Student t-test) between heavy rainfall and light rainfall.

## 4 Discussion

### 4.1 Factors responsible for moisture transport of heavy rainfall

Moisture flux into the HRV is mainly accomplished by large-scale atmospheric circulation associated with monsoon dynamics, i.e., the Indian monsoon and the East Asian summer monsoon (Zhou and Yu 2005), which collectively feed the HRV rainfall and affect the rainfall intensity (Zhou et al. 2020).

The comparison of moisture flux between heavy and light rainfall suggests that there is significantly more moisture carried by the increased southwesterly flow from South China to the HRV on the day of heavy rainfall (Fig. 7a). Prior to the heavy rainfall events, increased moisture flux from the Indian ocean and the southern subregion of the Pacific Ocean is observed compared with the light rainfall events (Fig. 7b). The increased moisture flux from the western Pacific plays a leading role only in the across-warp type of heavy rainfall (Zhou et al. 2020), and the abundant moisture carried by the low-latitude Indian monsoon is the main reason for most heavy rainfall events. The strong and stable westerly from Arabian Sea to Bay of Bengal (Yang et al. 2017) and the anomalous northeastward moisture flux to the south of 25° N caused by the active Indian monsoon low (Zhou et al. 2020) have been shown to affect the HRV heavy rainfall. Specifically, the northward moisture flux along the Somali jet is enhanced along with eastward flow over Arabian Sea, which deflect more moisture northward over Bay of Bengal and toward Southern China. As a result, excessive

moisture from the Indian Ocean is carried by the enhanced flow, and thus larger contribution to heavy rainfall than to light rainfall. These anomalous patterns of moisture flux are consistent with the WAM analysis (Figs. 5, 6).

Figure 7c shows that the wind distribution associated excessive evaporation over the Indian Ocean may be related to the increased moisture contribution from the Indian Ocean to HRV heavy rainfall. Compared to light rainfall, the wind of Somali jet and the eastward wind over the Arabian Sea are intensified before heavy rainfall although this intensification is seldom statistically significant. The increased evaporation promoted by the enhanced surface wind before heavy rainfall can also be found in the Indian Ocean, especially in the Arabian Sea with an average increase of about 0.3 mm day$^{-1}$. The intensified evaporation tends to moisten the air, resulting in more precipitable water. With the combination of dynamic and thermodynamic driving, more significant eastward and northeastward moisture transport anomalies are observed over the Indian Ocean (Fig. 7b), giving it great potential to influence the downwind regions. Facilitated by the lower tropospheric wind, these anomalies reach Southern China, where they are steered by the dynamic western Pacific subtropical high (WPSH) and guided into the HRV (Dong 2016; Li et al. 2016). Thus, the wind distribution connects excessive evaporation over the Indian Ocean and moisture flux into the HRV, making the Indian Ocean an especially important moisture source for heavy rainfall over the HRV.

### 4.2 Relevance and scientific significance of research

In addition to the direct effects of water vapor transport, many previous studies paid more attention to the impact of land-sea temperature contrast as well as the climate modes as mentioned in the introduction part. The atmospheric-ocean feedback mechanism usually has a great influence on moisture transport and rainfall (Gimeno et al. 2016). For instance, the negative-phase PDO can cause the East Asian monsoon anomaly (Wang et al. 2016; Zhang et al. 2007), and the negative-phase ENSO with the westward extension of WPSH will strengthen the connection with the southwesterly flux from the Indian Ocean (Hu et al. 2010; Wu et al. 2017). These certain phases can strengthen the meridional transport of moisture from the south and have been confirmed to trigger the increase in HRV summer rainfall (Wang et al. 2016; Zhang et al. 2007). Furthermore, during the positive-phase ENSO, the evaporation of Indian Ocean at low latitudes is still strong (Wu et al. 2017), and abundant moisture carried by the zonal low-level southwesterly flow anomaly provides heavy rainfall (Zhou et al. 2020). This indicates that our results on the difference between heavy rainfall and light rainfall are not entirely limited by specific periods of these patterns.

**Fig. 7** Differences in vertically integrated water vapor flux on the day of rainfall (**a**), and differences in climatological vertically integrated divergence of moisture flux (**b**) and climatological evaporation (**c**) between the traceback duration of heavy and light rainfall (heavy minus light). The shading is the difference in the magnitude of moisture flux divergence (**b**) or evaporation (**c**). The vector is the difference in the water vapor flux (**a**, **b**) or 850-hPa wind (**c**). The red arrow indicates the difference of data is statistically significant at the 0.05 level of Student t-test
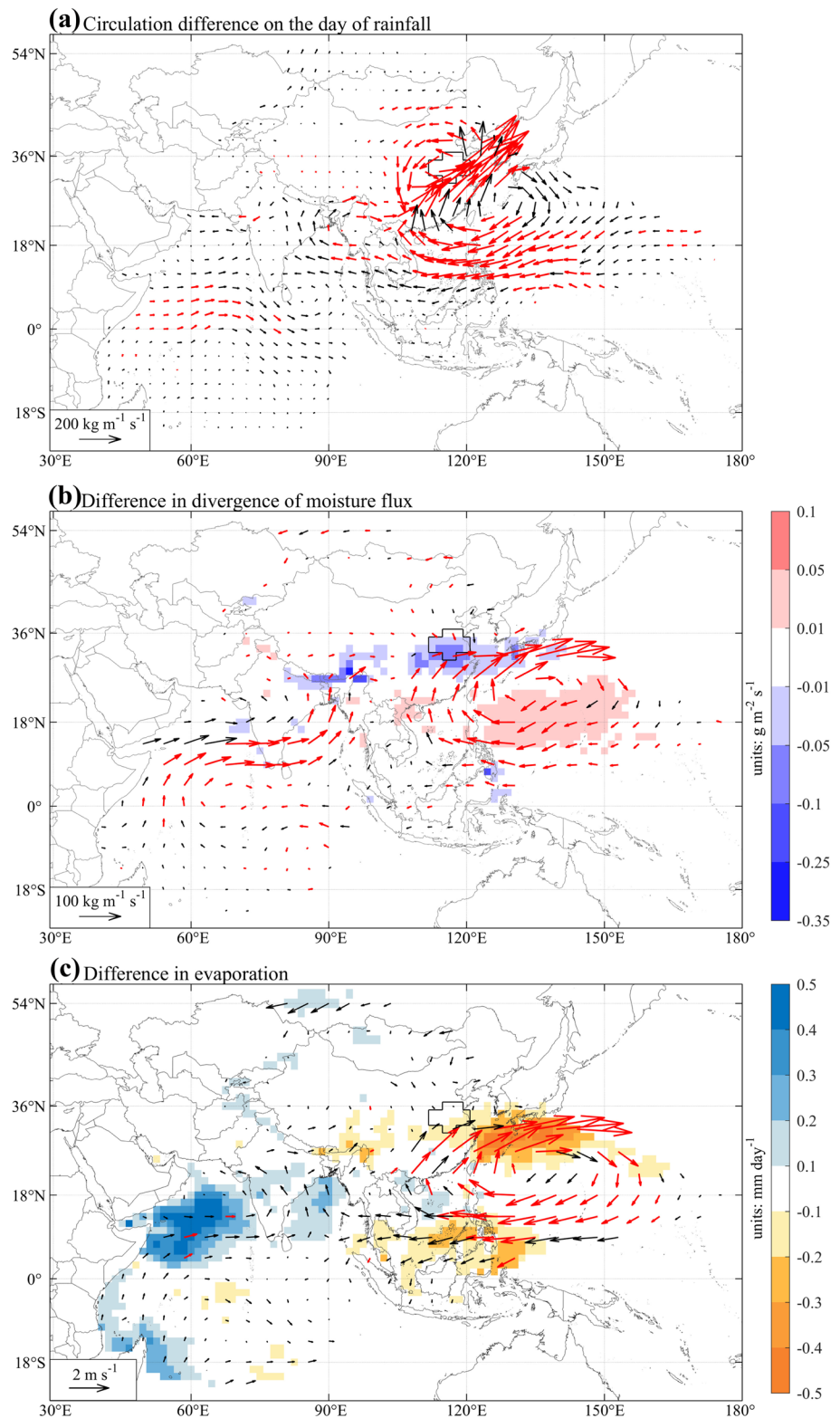


Climate factors and the physical processes involved are crucial in forecasting the variation of rainfall, however, the changes of the evaporation contribution from the source regions can provide us a new and more observable way to

try. Since the climate mode do not always have a significant impact on precipitation, the reference value of the moisture source contribution will be particularly important during the low-impact periods of the mode or the mode being the

same phase for a long time. As more moisture is transported from the subtropical ocean divergence zones to continental convergence zones (Gimeno et al. 2020a), the variation of hydrological links between the sources and sinks of heavy and extremely heavy rainfall deserves more attention. One thing to note is that, although we can use this as a method to predict changes in precipitation intensity in a general sense, the estimation results still cannot deviate from the prevailing meteorological and climatic conditions as well as the evolution of thermodynamics and dynamics.

The uncertainty of reanalysis precipitation data is discussed in Supplementary.

## 5 Conclusion

This study analyzed moisture sources for different rainfall intensity categories over the HRV during summer (JJA) from 1980 to 2018. Using the WAM model, moisture sources for HRV rainfall, their contributions and trends were identified. By analyzing the differences in each intensity category, the following conclusions are drawn:

1. The HRV summer rainfall is mainly (90%) supported by moistures from four regions, including the local HRV, the terrestrial subregion excluding the HRV, the Indian Ocean and the Pacific Ocean.
2. The moisture contribution ratios of the four sources vary with the HRV rainfall intensity. The local HRV evaporated moisture has a higher contribution ratio to light rainfall than heavy rainfall, whereas the moisture contribution from the Indian Ocean accounts for a larger proportion in heavy rainfall than in light rainfall.
3. The grids located in the north and south of the main moisture source region have different contribution to heavy rainfall and light rainfall. The portion of the moisture contribution evaporated from north (south) part is larger to light (heavy) rainfall than to heavy (light) rainfall over the HRV.

These results highlight the differences of moisture contribution of evaporation sources to different rainfall intensities in the HRV, which complements the existing understanding of the moisture supply over the HRV. Combined with previous studies, it better reflects the role of the moisture contribution from land and ocean in hydrological cycle and regional precipitation.

## References

Bosilovich MG (2002) On the vertical distribution of local and remote sources of water for precipitation. Meteorol Atmos Phys 80:31–41. https://doi.org/10.1007/s007030200012

Burde GI (2010) Bulk recycling models with incomplete vertical mixing. Part I: conceptual framework and models. J Clim 19:1461–1472. https://doi.org/10.1175/jcli3687.1

Dee DP, Uppala SM, Simmons AJ, Berrisford P, Poli P, Kobayashi S, Andrae U, Balmaseda MA, Balsamo G, Bauer P et al (2011) The ERA-Interim reanalysis: configuration and performance of the data assimilation system. Q J R Meteorol Soc 137:553–597. https://doi.org/10.1002/qj.828

Ding Y, Chan JCL (2005) The East Asian summer monsoon: an overview. Meteorol Atmos Phys 89:117–142. https://doi.org/10.1007/s00703-005-0125-z

Dong X (2016) Influences of the Pacific Decadal Oscillation on the East Asian Summer Monsoon in non-ENSO years. Atmos Sci Lett 17:115–120. https://doi.org/10.1002/asl.634

Drumond A, Nieto R, Gimeno L (2011) Sources of moisture for China and their variations during drier and wetter conditions in 2000–2004: a Lagrangian approach. Clim Res 50:215–225

Findell KL, Keys PW, Ent RJVD, Lintner BR, Berg A, Krasting JP (2019) Rising temperatures increase importance of oceanic evaporation as a source for continental precipitation. J Clim 32:7713–7726. https://doi.org/10.1175/jcli-d-19-0145.1

Fremme A, Sodemann H (2019) The role of land and ocean evaporation on the variability of precipitation in the Yangtze River valley. Hydrol Earth Syst Sci 23:2525–2540. https://doi.org/10.5194/hess-23-2525-2019

Gao G, Chen D, Xu Y (2008) Impact of climate change on runoff in the Huaihe River Basins. J Appl Meteorol Sci 19:741–748. https://doi.org/10.3724/SP.J.1011.2008.00323

Gimeno L, Nieto R, Drumond A, Castillo R, Trigo R (2013) Influence of the intensification of the major oceanic moisture sources on continental precipitation. Geophys Res Lett 40:1443–1450. https://doi.org/10.1002/grl.50338

Gimeno L, Dominguez F, Nieto R, Trigo R, Drumond A, Reason CJC, Taschetto AS, Ramos AM, Kumar R, Marengo J (2016) Major mechanisms of atmospheric moisture transport and their role in extreme precipitation events. Annu Rev Environ Resour. https://doi.org/10.1146/annurev-environ-110615-085558

Gimeno L, Nieto R, Sorí R (2020a) The growing importance of oceanic moisture sources for continental precipitation. Clim Atmos Sci 3:27. https://doi.org/10.1038/s41612-020-00133-y

Gimeno L, Vázquez M, Eiras-Barca J, Sorí R, Stojanovic M, Algarra I, Nieto R, Ramos AM, Durán-Quesada AM, Dominguez F (2020b) Recent progress on the sources of continental precipitation as revealed by moisture transport analysis. Earth Sci Rev 201:103070. https://doi.org/10.1016/j.earscirev.2019.103070

Goessling HF, Reick CH (2013) On the "well-mixed" assumption and numerical 2-D tracing of atmospheric moisture. Atmos Chem Phys 13:5567–5585. https://doi.org/10.5194/acp-13-5567-2013

Guo L, Klingaman NP, Demory M-E, Vidale PL, Turner AG, Stephan CC (2018) The contributions of local and remote atmospheric moisture fluxes to East Asian precipitation and its variability. Clim Dyn 51:4139–4156. https://doi.org/10.1007/s00382-017-4064-4

Gustafsson M, Rayner D, Chen DL (2010) Extreme rainfall events in southern Sweden: where does the moisture come from? Tellus Ser A Dyn Meteorol Oceanogr 62:605–616. https://doi.org/10.1111/j.1600-0870.2010.00456.x

Hao L, and Zhao L (2014) Analysis on the climate characteristics of rainstorm weather over Huai River Basin and its influence on agriculture production. J Anhui Agric Sci:8662–8664

Hu Z, Wu R, Kinter JL, Yang S (2010) Connection of summer rainfall variations in South and East Asia: role of El Nino-southern oscillation. Int J Climatol 25:1279–1289

Huang R, Huang G, Wei Z (2004) Climate variations of the summer monsoon over China. Clim Dyn. https://doi.org/10.1142/978981 2701411_0006

Insua-Costa D, Miguez-Macho G (2018) A new moisture tagging capability in the Weather Research and Forecasting model: formulation, validation and application to the 2014 Great Lake-effect snowstorm. Earth Syst Dynam 9:167–185. https://doi.org/10.5194/esd-9-167-2018

Jiang Z, Ren W, Liu Z, Yang H (2013) Analysis of water vapor transport characteristics during the Meiyu over the Yangtze–Huaihe River valley using the Lagrangian method. Acta Meteor Sin 71:295–304

Jiang Z, Shuai J, Yi S, Liu Z, Wei L, Li L (2017) Impact of moisture source variation on decadal-scale changes of precipitation in North China from 1951 to 2010: moisture source variation. J Geophys Res 122:600–613. https://doi.org/10.1002/2016JD025795

Li M, Lv H, Ouyang F (2012) Analysis and prediction of climate change in Huaihe River Basin based on Delta method. Yangtze River 43:11-14+46. https://doi.org/10.16232/j.cnki.1001-4179.2012.07.001

Li L, Li W, Tang Q, Zhang P, Liu Y (2016) Warm season heavy rainfall events over the Huaihe River Valley and their linkage with wintertime thermal condition of the tropical oceans. Clim Dyn 46:71–82. https://doi.org/10.1007/s00382-015-2569-2

Liu X, Song XF, Xia J, Jing jie YU, and Zhang XC (2007) Characteristics of hydrogen and oxygen isotopes and preliminary analysis of vapor source for precipitation in chabagou catchment of the Loess Plateau. Resour Sci

Nieto R, Ciric D, Vázquez M, Liberato MLR, Gimeno L (2019) Contribution of the main moisture sources to precipitation during extreme peak precipitation months. Adv Water Resour. https://doi.org/10.1016/j.advwatres.2019.103385

Pathak A, Ghosh S, Martinez JA, Dominguez F, Kumar P (2016) Role of oceanic and land moisture sources and transport in the seasonal and inter-annual variability of summer monsoon in India. J Clim. https://doi.org/10.1175/JCLI-D-16-0156.1

Stohl A, James P (2004) A Lagrangian analysis of the atmospheric branch of the global water cycle. Part I: method description, validation, and demonstration for the August 2002 flooding in Central Europe. J Hydrometeorol 5:656

Stohl A, James P (2005) A Lagrangian analysis of the atmospheric branch of the global water cycle. Part II: moisture transports between earth's ocean basins and river catchments. J Hydrometeorol 6:961–984

Tang Q (2020) Global change hydrology: terrestrial water cycle and global change. Sci China Earth Sci 63:459–462

Trenberth KE (1998) Atmospheric moisture residence times and cycling: implications for rainfall rates and climate change. Clim Change 39:667–694. https://doi.org/10.1023/A:1005319109110

Trenberth KE (1999) Atmospheric moisture recycling: role of advection and local evaporation. J Clim 12:1368–1381. https://doi.org/10.1175/1520-0442(1999)012%3c1368:AMRROA%3e2.0.CO;2

Trenberth KE, Dai A, Rasmussen RM, Parsons DB (2010) The changing character of precipitation. Bull Am Meteorol Soc 84:1205–1217. https://doi.org/10.1175/BAMS-84-9-1205

Trenberth KE, Fasullo JT, Mackaro J (2011) Atmospheric moisture transports from ocean to land and global energy flows in reanalyses. J Clim 24:4907–4924. https://doi.org/10.1175/2011JCLI4171.1

van der Ent RJ, Savenije HHG (2011) Length and time scales of atmospheric moisture recycling. Atmos Chem Phys 11:1853–1863. https://doi.org/10.5194/acp-11-1853-2011

van der Ent RJ, Savenije HHG, Schaefli B, Steele-Dunne SC (2010) Origin and fate of atmospheric moisture over continents. Water Resour Res. https://doi.org/10.1029/2010WR009127

van der Ent RJ, Tuinenburg OA, Knoche HR, Kunstmann H, Savenije HHG (2013) Should we use a simple or complex model for moisture recycling and atmospheric moisture tracking? Hydrol Earth Syst Sci 17:4869–4884. https://doi.org/10.5194/hess-17-4869-2013

Wang Y, Zhang Q, Gu X, Kong D (2016) Summer precipitation in the Huaihe river basins and relevant climate indices. J Appl Meteorol Sci 27:67–74

Wu D, Yan D (2013) Projections of future climate change over Huaihe River basin by bultimodel ensembles under SRES scenarios. J Lake Sci 25:565–575. https://doi.org/10.18307/2013.0415

Wu P, Ding Y, Liu Y (2017) A new study of El Nino impacts on summertime water vapor transport and rainfall in China. Acta Meteorol Sin:371–383

Yang W, Xu M, Zhou S, Luo L (2017) Spatial-temporal variation of extreme precipitation events from June to July over Yangtze-Huaihe river basin and the circulation anomalies. Plateau Meteorol 36:718–735

Yoshimura K, Oki T, Ohte N, Kanae S (2004) Colored moisture analysis estimates of variations in 1998 Asian monsoon water sources. J Meteorol Soc Jpn 82:1315–1329. https://doi.org/10.2151/jmsj.2004.1315

Zhang C, Li Q (2014) Tracking the moisture sources of an extreme precipitation event in Shandong, China in July 2007: a computational analysis. J Meteorol Res 28:634–644. https://doi.org/10.1007/s13351-014-3084-9

Zhang YL, You WJ (2014) Social vulnerability to floods: a case study of Huaihe River Basin. Nat Hazards 71:2113–2125. https://doi.org/10.1007/s11069-013-0996-0

Zhang J, Zhu W, Li Z (2007) Relationship beteen winter North Pacific Oscillations and summer precipitation anomalies in the Huaihe River Basin. J Nanjing Inst Meteorol 030:546–550

Zhang C, Tang Q, Chen D (2017) Recent changes in the moisture source of precipitation over the Tibetan Plateau. J Clim 30:1807–1819. https://doi.org/10.1175/JCLI-D-15-0842.1

Zhang C, Tang Q, Chen D, van der Ent RJ, Liu X, Li W, Haile GG (2019) Moisture source changes contributed to different

precipitation changes over the Northern and Southern Tibetan Plateau. J Hydrometeorol 20:217–229. https://doi.org/10.1175/jhm-d-18-0094.1

Zhao Y, Zhu J, Xu Y (2014) Establishment and assessment of the grid precipitation datasets in China for recent 50 years. J Meteorol Sci 34:414–420

Zhou T, Yu R (2005) Atmospheric water vapor transport associated with typical anomalous summer rainfall patterns in China. J Geophys Res Atmos 110:D08104

Zhou X, Sun J, Zhang L, Chen G, Cao J, Jie B (2020) Classification characteristics of continuous extreme rainfall events in North China. Acta Meteorol Sin

**Publisher's Note** Springer Nature remains neutral with regard to jurisdictional claims in published maps and institutional affiliations.